

Retraction

Retracted: Hemodynamic-Based Evaluation on Thrombosis Risk of Fusiform Coronary Artery Aneurysms Using Computational Fluid Dynamic Simulation Method

Complexity

Received 23 January 2024; Accepted 23 January 2024; Published 24 January 2024

Copyright © 2024 Complexity. This is an open access article distributed under the Creative Commons Attribution License, which permits unrestricted use, distribution, and reproduction in any medium, provided the original work is properly cited.

This article has been retracted by Hindawi following an investigation undertaken by the publisher [1]. This investigation has uncovered evidence of one or more of the following indicators of systematic manipulation of the publication process:

- (1) Discrepancies in scope
- (2) Discrepancies in the description of the research reported
- (3) Discrepancies between the availability of data and the research described
- (4) Inappropriate citations
- (5) Incoherent, meaningless and/or irrelevant content included in the article
- (6) Manipulated or compromised peer review

The presence of these indicators undermines our confidence in the integrity of the article's content and we cannot, therefore, vouch for its reliability. Please note that this notice is intended solely to alert readers that the content of this article is unreliable. We have not investigated whether authors were aware of or involved in the systematic manipulation of the publication process.

Wiley and Hindawi regrets that the usual quality checks did not identify these issues before publication and have since put additional measures in place to safeguard research integrity.

We wish to credit our own Research Integrity and Research Publishing teams and anonymous and named external researchers and research integrity experts for contributing to this investigation.

The corresponding author, as the representative of all authors, has been given the opportunity to register their agreement or disagreement to this retraction. We have kept a record of any response received.

References

- [1] H. Wang, H. Anzai, Y. Liu, A. Qiao, J. Xie, and M. Ohta, "Hemodynamic-Based Evaluation on Thrombosis Risk of Fusiform Coronary Artery Aneurysms Using Computational Fluid Dynamic Simulation Method," *Complexity*, vol. 2020, Article ID 8507273, 11 pages, 2020.

Research Article

Hemodynamic-Based Evaluation on Thrombosis Risk of Fusiform Coronary Artery Aneurysms Using Computational Fluid Dynamic Simulation Method

Haoran Wang,^{1,2} Hitomi Anzai,¹ Youjun Liu,³ Aike Qiao ,³ Jinsheng Xie,⁴ and Makoto Ohta ^{1,5}

¹Institute of Fluid Science, Tohoku University, 2-1-1, Katahira, Aoba-Ku, Sendai, Miyagi 980-8577, Japan

²Graduate School of Biomedical Engineering, Tohoku University, 6-6 Aramaki-Aza-Aoba, Aoba-Ku, Sendai, Miyagi 980-8579, Japan

³College of Life Science and Bioengineering, Beijing University of Technology, No. 100 Pingleyuan, Chaoyang District, Beijing 100022, China

⁴Department of Cardiac Surgery, Beijing Anzhen Hospital Capital Medical University, Beijing Institute of Heart Lung and Blood Vessel Diseases, Beijing 100029, China

⁵ELyTMax UMI 3757, CNRS-Université de Lyon, Tohoku University, Sendai, Japan

Correspondence should be addressed to Makoto Ohta; ohta@biofluid.ifs.tohoku.ac.jp

Received 15 May 2020; Revised 13 July 2020; Accepted 20 July 2020; Published 20 October 2020

Guest Editor: Zhihan Lv

Copyright © 2020 Haoran Wang et al. This is an open access article distributed under the Creative Commons Attribution License, which permits unrestricted use, distribution, and reproduction in any medium, provided the original work is properly cited.

Coronary artery aneurysms (CAAs) have been reported to associate with an increased risk for thrombosis. Distinct to the brain aneurysm, which can cause a rupture, CAA's threat is more about its potential to induce thrombosis, leading to myocardial infarction. Case reports suggest that thrombosis risk varied with the different CAA diameters and hemodynamics effects (usually wall shear stress (WSS), oscillatory shear index (OSI), and relative residence time (RRT)) may relate to the thrombosis risk. However, currently, due to the rareness of the disease, there is limited knowledge of the hemodynamics effects of CAA. The aim of the study was to estimate the relationship between hemodynamic effects and different diameters of CAAs. Computational fluid dynamics (CFD) provides a noninvasive means of hemodynamic research. Four three-dimensional models were constructed, representing coronary arteries with a normal diameter (1x) and CAAs with diameters two (2x), three (3x), and five times (5x) that of the normal diameter. A lumped parameter model (LPM) which can capture the feature of coronary blood flow supplied the boundary conditions. WSS in the aneurysm decreased 97.7% apparently from 3.51 Pa (1x) to 0.08 Pa (5x). OSI and RRT in the aneurysm were increased apparently by two orders of magnitude from 0.01 (1x) to 0.30 (5x), and from 0.38 Pa⁻¹ (1x) to 51.59 Pa⁻¹ (5x), separately. Changes in the local volume of the CAA resulted in dramatic changes in local hemodynamic parameters. The findings demonstrated that thrombosis risk increased with increasing diameter and was strongly exacerbated at larger diameters of CAA. The 2x model exhibited the lowest thrombosis risk among the models, suggesting the low-damage (medication) treatment may work. High-damage (surgery) treatment may need to be considered when CAA diameter is 3 times or higher. This diameter classification method may be a good example for constructing a more complex hemodynamic-based risk stratification method and could support clinical decision-making in the assessment of CAA.

1. Introduction

A coronary artery aneurysm (CAA) is a localized swelling in one of the coronary arteries that supply oxygen to the heart. It is typically defined by a diameter at least 1.5 times that of

the adjacent normal segments of the artery. It is called the giant CAA when the diameter of a CAA exceeds four times the diameter of its adjacent coronary artery [1]. The incidence of CAAs has been reported as 0.3%-5.3% [2]. However, the prevalence of CAA in different literature varies due

to statistical data, [3–6], lack of standardization for diagnosis on angiography [5, 7], and different CAA definitions [8]. CAA is generally associated with the risk of complications such as infarction, ischemia, and thrombosis, with the thrombosis being the most common [9]. Unlike other types of aneurysms, which pose a risk of rupture, the main risk caused by CAA is thrombosis rather than rupture [1].

Current American Heart Association (AHA) guidelines for risk stratification rely on aneurysm size alone as the criterion for initiating systemic anticoagulation; however, studies suggest risk may also depend on hemodynamic parameters such as low wall shear stress (WSS), high oscillatory shear index (OSI), and high relative residence time (RRT), which are not available through image data alone [10–13]. Indeed, CAAs' complex geometries, such as the diameter, may contribute to abnormal hemodynamics and correlate with patient outcome. Considering the other risks, doctors may be confused about the dilemma of whether to adopt the watch-and-wait approach, with the risk of sudden deterioration, or to expose the patient to the risks of treatment if just based on the image data alone. Therefore, it is necessary to evaluate the relationship between CAA diameter and level of thrombosis risk based on the hemodynamic study which could provide support for the doctors.

Patient-specific hemodynamic simulations by using computational fluid dynamics (CFD) can non-invasively supply informative hemodynamic parameters for better thrombotic risk assessment; however, existing studies have been limited and struggle to quantify effects of aneurysm shape on local hemodynamics. With such limitations in mind, existing patient-specific models can be augmented by introducing artificial aneurysms of specified diameter, to achieve a systematic evaluation of the relationship between CAA size and the local hemodynamics. Ultimately, elucidating the relationship between hemodynamics and aneurysmal size characteristics may underlie more powerful risk stratification methods to support clinical decision-making. Usually, these treatments include high-risk surgical treatment and conservative treatment regarding initiation of anticoagulant therapy. Surgery has multiple risks such as the risk of anesthesia, postoperative complications, and the like. Due to the large changes in the cardiovascular structure of the operation, even if the surgical operation has complete risk management, some postoperative complications such as weakened cardiac function and arrhythmia cannot be completely avoided.

CFD has been used widely in the research of vascular diseases in recent years [14–16] and can be used to estimate important hemodynamic parameters including mass flow, WSS, OSI, and RRT. The mass-flow rate can usually be calculated based on speed measurement using non-invasive ultrasonic velocimetry. However, other parameter, WSS, OSI, and RRT, measurements are much more complicated and cannot be accurately measured directly. The indirect calculation method of in vitro experiments, which means the need to build an experimental system and need to consider every potential problem in the system, also has high cost. The advantages of CFD, such as gaining insight into systems that might be difficult to test through

experimentation and lower costs, can overcome the shortcomings of other measurement methods mentioned above. Simulations have played important roles in other studies, such as bypass grafts [17, 18] and abdominal and cerebral aneurysms [19–21], but this technique has rarely been applied to CAAs. One of the important factors is that the characteristics of the coronary artery make its simulation difficult. In the human physiological environment, the resistance of the coronary arteries changes repeatedly; during systole, the resistance of the coronary circulation increases considerably due to the contraction of the heart. In contrast, during diastole, the pressure decreases, which reduces coronary microcirculation resistance. As a consequence, the coronary blood supply increased. In order not to lose the characteristics of the coronary artery, we have adopted a circuit model called lumped parameter model (LPM) to simulate the coronary artery to provide the boundary conditions for the CFD simulation work [22].

The aim of the study was to estimate the relationship between hemodynamic effects and different diameter of CAAs. We quantified hemodynamic parameters of likely clinical relevance for assessing the thrombotic risk including WSS, OSI, and RRT. We created virtual models by artificially constructing models of normal coronary and different diameter of CAAs to compare normal and pathological hemodynamics. This study will allow us to estimate the risk of thrombosis of CAAs from a hemodynamic perspective and provide more comprehensive support for doctors' decisions.

2. Materials and Methods

2.1. Model Development and Simulation Methods. A patient-specific anatomy model was constructed, based on patient data provided by Anzhen Hospital. All patient information for this analysis was anonymized. This study has been approved by the Medical Ethics Committee of Beijing Anzhen Hospital and Tohoku University. The images used for the 3D model reconstruction were obtained by CT. A personalized real 3D anatomic geometry model was built with manual and threshold segmentation by using Mimics processing software (Materialise NV, Leuven, Belgium). The single fusiform CAAs of different diameters were added to the left anterior descending artery by using the PHANTOM Desktop in Freeform software (3D Systems, USA). We have only changed the diameter of CAA and have not changed the length of CAA along the coronary artery. The link between CAA and normal coronary artery was smoothed. All the changes have been confirmed by the medical doctor. CAA models were constructed with diameters two, three, and five times that of the normal segments of the coronary artery, as well as a model of a normal coronary artery without an aneurysm (Models 2x, 3x, and 5x, respectively; Figure 1), so that we can study hemodynamics on both regular and giant size (Figure 1).

The computational models were generated by 3D model meshing, using a hexahedral mesh controlled by size control using ANSYS Meshing software (Swanson Analysis Systems, Inc., USA). The grids of the regions local to the CAA were refined to allow more precise simulation calculations in these areas for more accurate results.

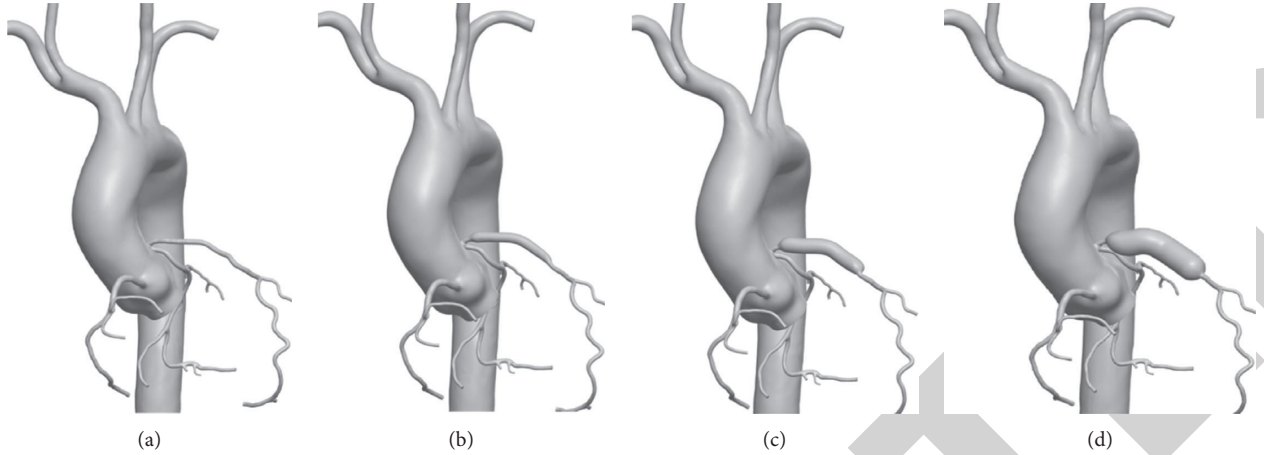


FIGURE 1: Three-dimensional models with a normal coronary artery (Model 0) and with coronary artery aneurysms with diameters two, three, and five times that of the normal diameter (Models 2x, 3x, and 5x, respectively). (a) Model 0. (b) Model 2x. (c) Model 3x. (d) Model 5x.

To confirm the reliability of the simulation results, we performed a grid independence test on the number of elements and nodes [22]. See Figure 2 to check more information of the independence test. It can be found that the simulation results tend to be stable when the number of grids exceeds a certain standard. The total numbers of nodes and elements for the four models differed (Table 1), but they were all of the same order of magnitude number. Blood flow simulations were performed by using the Navier–Stokes solver in the ANSYS-CFX software (Swanson Analysis Systems, Inc.). The simulation calculation assumed that the artery wall was rigid and stationary, the blood flow was Newtonian, and the density and viscosity were 1050 kg/m^3 and 0.0035 Pa s , respectively. Based on the Reynolds number, the fluid is set as laminar flow. The simulations were run for three cardiac cycles. We selected a time step of 0.0025 s to satisfy the calculation of stability conditions. The maximum residual of momentum and continuity of the iterative calculation was set to 0.0001 .

2.2. Lumped Parameter Boundary Conditions. The coronary artery blood flow simulation required careful consideration of the physiological function of the coronary circulation and microcirculation, especially the drastic change in microcirculatory resistance due to heart contractions. This could be simulated appropriately by using an LPM. The LPM construction method for the boundary conditions was based on previous research [22, 23]. The LPM system comprised a heart left ventricle module, coronary artery modules, and arterial modules. These modules were developed based on the concept of the three-element Windkessel RCR (resistor-capacitor-resistor) model [24], a simple circuit model in which blood flow and blood pressure were considered to be analogous to electrical current and voltage, and the resistance and compliance of blood vessels were characterized by resistance and capacitance, respectively. The entire multiscale model is shown in Figure 3. The heart module can be built using some components such as power source and variable capacitor on the basis of the RCR model. The power can simulate the

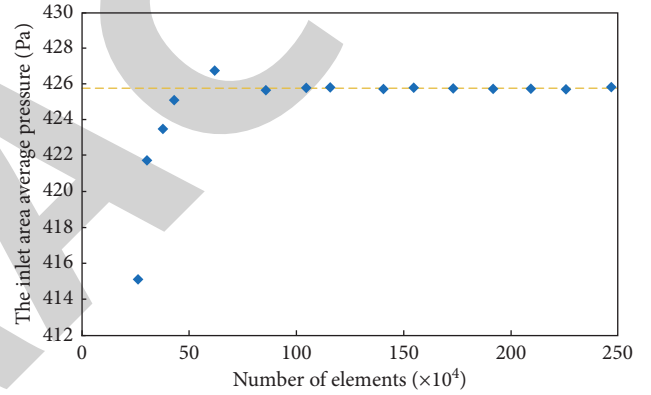


FIGURE 2: The result of grid independence test and the trend line of the results.

TABLE 1: The numbers of nodes and elements of the grid in the four computational models.

	Model 0	Model 2x	Model 3x	Model 5x
Nodes	1,098,996	940,577	1,047,183	936,749
Elements	1,437,901	1,231,913	1,370,433	1,230,434

blood pressure and the variable capacitor can simulate the volume change of the ventricular during the systole and diastole. The inlet flow via the ascending aorta was provided by the LPM heart module, and the LPM heart model was connected to the LPM coronary artery models through intramyocardial pressure. The components of this module included resistors, capacitors, inductors, and diodes, which were used to simulate coronary resistance, vascular compliance, blood flow inertia, and the heart valves, respectively. The pressure–volume relationship representing the vascular compliance was calculated as follows:

$$C(t) = \frac{V(t) - V_0}{P(t)} = \frac{1}{E(t)}, \quad (1)$$

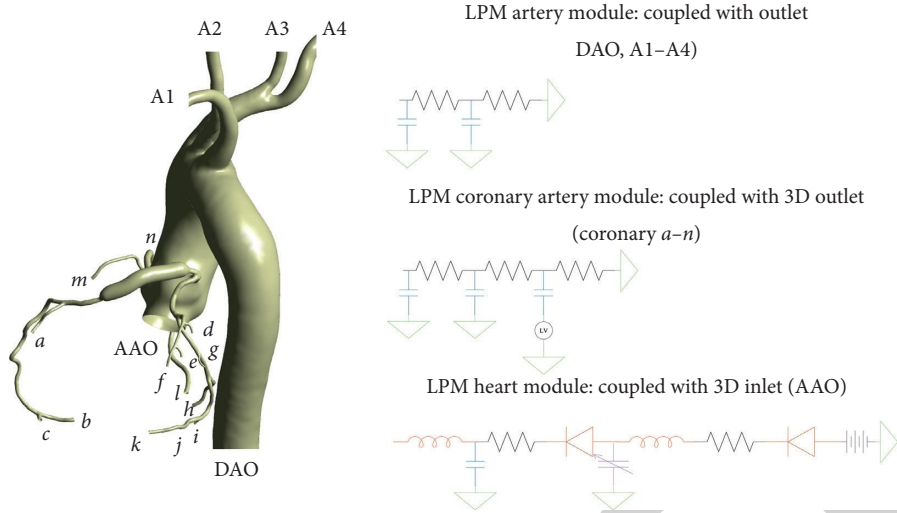


FIGURE 3: Details of the multiscale model used in the study, showing the coupled interface between the lumped parameter model (LPM) and the three-dimensional model. *an*, coronary arteries; A1A4, arteries; AAO, ascending aorta; DAO, descending aorta; RCR, resistor-capacitor-resistor.

where $V(t)$ and $P(t)$ are the pressure and volume of the ventricle and V_0 is the reference pressure. $E(t)$ characterizes the time-varying elastic properties and was calculated as follows:

$$E(t) = E_{\min} + (E_{\max} - E_{\min}) \cdot E_n(t_n). \quad (2)$$

The units of E used were mL and mmHg. Normalized time-varying elasticity $E_n(t_n)$ was calculated using a method based on previous research [25] as follows:

$$E_n(t_n) = 1.55 \left[\frac{1}{1 + (t_n/1.17)^{21.9}} \right] \left[\frac{(t_n/0.7)^{1.9}}{1 + (t_n/0.7)^{1.9}} \right]. \quad (3)$$

In the present study, we set $E_{\min} = 0.002458$ and $E_{\max} = 2.0$. $t_n = (t/(0.2 + 0.15t_c))$. The cardiac cycle t_c was set to 0.8 s.

Compared with normal arterial blood vessels, the coronary artery module required the addition of a microcirculation module to take account of the special physiology of coronary arteries. This module comprised a resistor ($R_{v\text{-micro}}$) and a capacitor ($C_{i\text{-micro}}$), with the cathode of the capacitor coupled to the internal pressure of the heart module to simulate changes in systolic pressure. The target mean flow of every branch of the LPM coronary arteries was determined by the area of each branch [23, 26]. Based on previous studies [22, 27], we assumed that the total perfusion of the coronary arteries was 4% of the cardiac output and that the total perfusion of the left and right coronary arteries was 60% and 40% of the total perfusion of the coronary arteries, respectively. As shown in Figure 2, the simulation of coronary microcirculation is to add a module on the basis of the common artery to simulate the pressure from the left ventricle and the resistance change caused by the pressure change. The debugging of the entire circuit model parameters is based on previous research [22], in which the pressure adjustment needs to match the patient's blood pressure.

The RCR model can be used to directly simulate arterial blood vessels because these do not undergo drastic changes in resistance. The RCR boundary conditions were set as the outlets of the descending aorta and supra-aortic arteries.

The CFD boundary conditions provided by the LPM for the inlet and outlets of the computational model corresponded to different modules, known as the 0D/3D multiscale coupled method [22, 23]. The important reasons for adopting LPM are the easy-to-deploy circuit model and the characteristics of not requiring a mainframe computer. The easy-to-deploy circuit model means that a complex circuit model composed of many different components can be simulated by programming. All four 3D models shared the same LPM, because, apart from the CAA lesion, the peripheral vascular geometry did not change between the models; this ensured changes in the geometric structure of the CAA were the main cause of the different simulation results. Clinical observation has shown that the coronary structure of the distal end of the coronary artery is not affected by the CAA; this was important evidence supporting the selection of this method.

3. Results

3.1. Mass Flow and Pressure Waveforms. Figure 4 shows the computed mass flow and pressure over a cardiac cycle for the ascending aorta (the inlet to the model), the descending aorta, an outlet artery, and a coronary artery branch (examples of outlets from the model) for the four 3D models. The results confirmed that, except for the mass flow at the coronary artery boundary, mass flow in the outlets peaked during systole. The coronary mass flow peaked during diastole. These results confirmed that the expected life-like characteristics of the coronary circulation, which blood supply mainly occurred during diastole, were successfully captured in the model [22]. High systolic intra-myocardial pressure resulted in increased distal downstream resistance

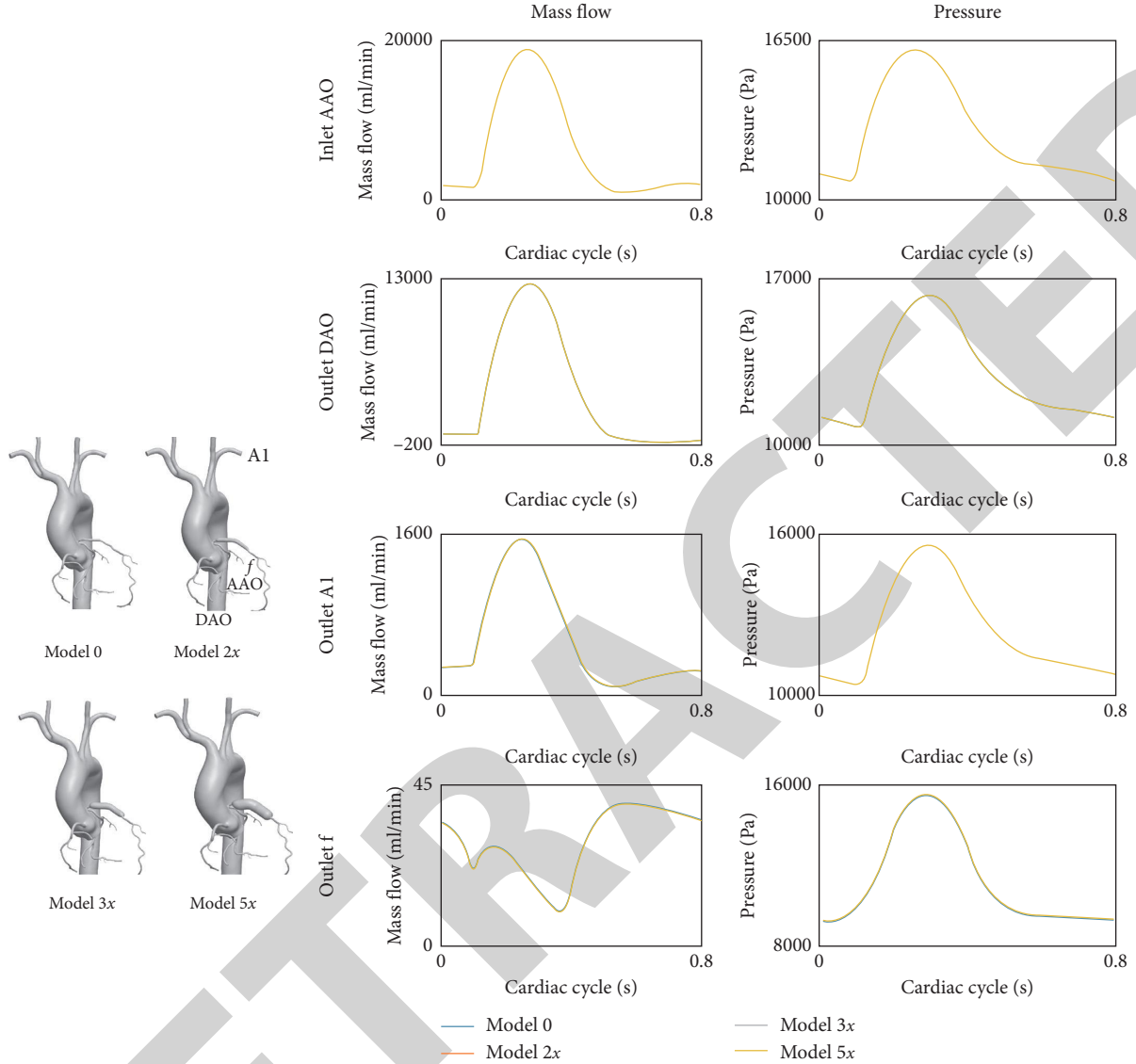


FIGURE 4: Mass flow and pressure curves for the inlet (ascending aorta, AAO) and three outlets (descending aorta (DAO), artery 1 (A1), and coronary artery f) over a cardiac cycle.

and decreased blood flow through the coronary artery; the opposite was the case during diastole. Changes in the diameter of the CAA did not have a significant effect on coronary outlet flow.

3.2. Wall Shear Stress. The WSS is the force per unit area exerted by the wall on the fluid in a direction along the plane of the local tangent [28], calculated as follows:

$$\tau_w = \frac{4\mu Q}{\pi R^3}, \quad (4)$$

where μ represents the blood viscosity, Q is mass-flow rate, and R is vessel radius. Previous studies have reported an association between thrombosis formation and low WSS [29]. The area average values of WSS in coronary artery aneurysm over a cardiac cycle in the four models

are listed in Table 2, and the values over a cycle and distribution contours are shown in Figures 5 and 6. The average WSS over a cycle in Model 0 (with no CAA) was 3.51 Pa. The averages for Models 2x, 3x, and 5x were 0.68, 0.26, and 0.08 Pa, respectively, substantially reduced in the CAA due to blood flow stagnation and recirculation, with the reduction increasing in CAAs of greater diameters. The distribution contours in Figure 6 confirm that the CAA results only in local hemodynamic disturbances without wider hemodynamic changes in the arteries. At some distance downstream in the coronary artery, the coronary diameter and WSS both return to normal levels.

3.3. Oscillatory Shear Index. OSI is a parameter that quantifies the magnitude of the WSS and directional changes [18], calculated as follows:

TABLE 2: Average values over a cardiac cycle for wall shear stress (WSS), the oscillatory shear index (OSI), and relative residence time (RRT) in the coronary artery aneurysm.

	Model 0	Model 2x	Model 3x	Model 5x
Area average WSS (Pa)	3.51	0.68	0.26	0.08
Area average OSI	0.01	0.03	0.13	0.30
Area average RRT (Pa ⁻¹)	0.38	2.88	23.12	51.59

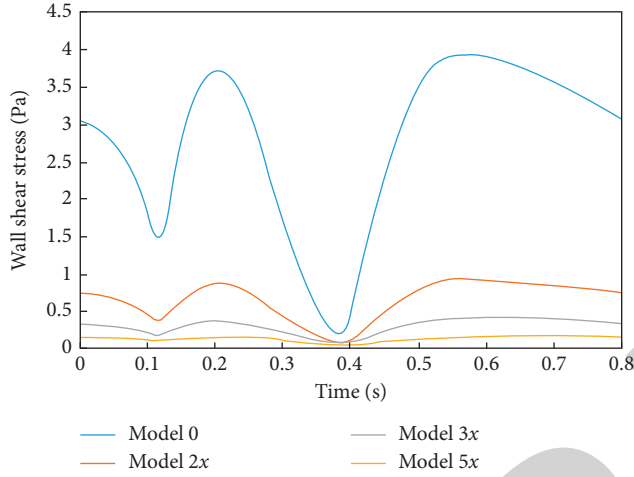


FIGURE 5: Wall shear stress in the coronary artery aneurysm over a cardiac cycle for the four models.

$$\text{OSI} = 0.5 \times \left(1 - \frac{\left| \int_0^T \tau_w dt \right|}{\int_0^T |\tau_w| dt} \right), \quad (5)$$

where T is the cardiac cycle. OSI has values in the range 0.0 to 0.5, with 0 representing undisturbed flow with no change in the direction of the shear stress and 0.5 representing disturbed flow with oscillating shear stress. Previous studies have reported an association between high OSI and the formation of intimal hyperplasia [30]. The average values of OSI in the aneurysm and OSI distribution contours are shown in Table 2 and Figure 7, respectively. The average value of OSI over the cardiac cycle in Model 0 was 0.01. The averages for Models 2x, 3x, and 5x were substantially higher, at 0.03, 0.13, and 0.30, respectively. Previous studies have pointed out that when OSI is greater than 0.2, it will cause endothelial cell damage [31]. As shown in Table 3, the ratio of high OSI area in the aneurysm to the area of aneurysm was 0%, 12.5%, 25.3%, and 66.2%, respectively. Model 0 has OSI close to zero throughout the cardiac cycle, and the flow in Model 0 is unidirectional without circulation. Normal coronary blood flow is unidirectional, usually without flow recirculation, so the OSI of the normal coronary artery (Model 0) was close to zero throughout the entire cardiac cycle. The high OSI values in the CAA models, which reached 30 times higher in model 5x, were due to the increased storage time resulting from the increased size of the cavity, which led to recirculation within the CAA lesion. The effect on OSI was locally confined; there

was little difference between the OSI in the distal coronary arteries in Models 2x, 3x, and 5x and those in Model 0.

3.4. Relative Residence Time. The RRT is an indicator that comprehensively characterizes the values and oscillation of WSS [32], as well as the time of local blood flow and vascular interaction [33]. It is calculated as follows:

$$\text{RRT} = \frac{1}{(1 - 2 \cdot \text{OSI}) \cdot \text{TAWSS}}, \quad (6)$$

where

$$\text{TAWSS} = \frac{\text{WSS}}{T}. \quad (7)$$

Here, TAWSS is WSS average over one cardiac cycle, and T is a cardiac cycle. Figure 8 shows the distribution contours for RRT in the four models, and Table 2 shows the area average values of RRT within the CAA lesion over the cardiac cycle. The average value of RRT in Model 0 was 0.38 Pa⁻¹. The averages for Models 2x, 3x, and 5x were substantially higher, at 2.88, 23.12, and 51.59 Pa⁻¹, respectively, showing a dramatic increase in RRT with increasing diameter of the CAA. Studies have reported a significantly increased risk of thrombosis when RRT is >10 Pa⁻¹ [12, 34]. As shown in Table 3, the ratio of high RRT area in the aneurysm to the area of aneurysm was 0%, 0.5%, 27.1%, and 78.6%, respectively. The increased diameter of the CAA makes it easier for blood to remain resident within it, hampering the blood flow to the distal coronary artery. The change in RRT was locally confined to the CAA; there was little difference between the RRT in the distal coronary arteries in Models 2x, 3x, and 5x and that in the distal coronary artery in Model 0.

4. Discussion

We have shown that the relationship between hemodynamic effects and different diameters of CAAs can be achieved by using CFD simulation method direct comparison with virtual control case based on the same patient. We found that changes in the diameter of CAA have a strong effect on local hemodynamics while they do not have a significant effect on global hemodynamics. The potential risk of thrombosis increases significantly with increasing CAA diameter indicated through decreasing WSS, increasing OSI and RRT. This research will allow us to estimate the thrombosis risk of CAAs from a hemodynamic perspective and provide more comprehensive support for doctors' decisions.

When making treatment decisions about CAAs, doctors typically depend on their own clinical experience [35]. This may be because of the lack of useful diagnostic tools. The current used tool is the method of imaging which can provide geometric information and almost no other information. The lack of other information cannot provide more help for the doctor's diagnosis. Therefore, it is necessary to find a way to provide more information to help the doctor. It has been shown that WSS over aneurysmal regions is

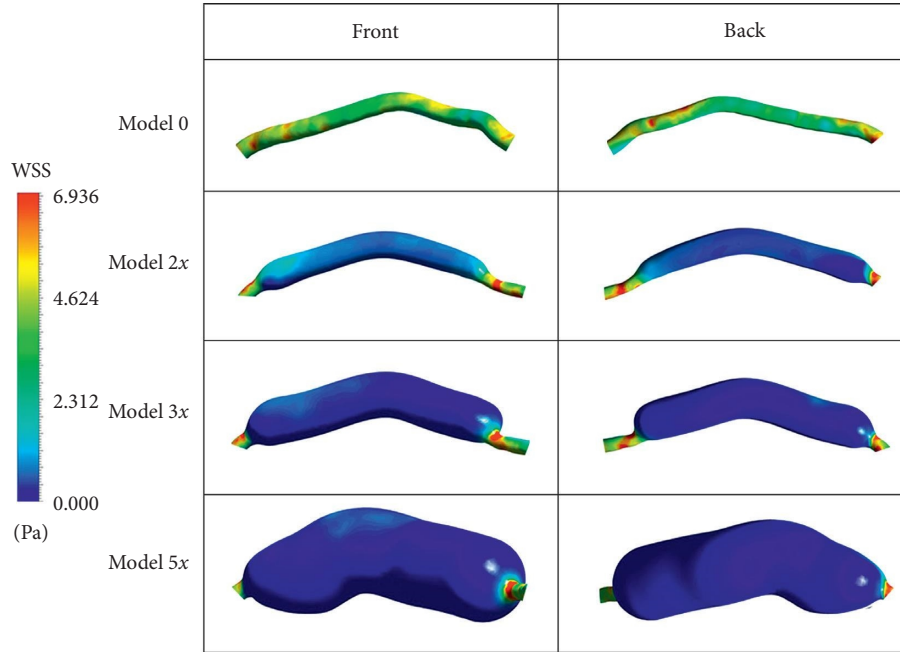


FIGURE 6: Wall shear stress (WSS) distribution in the coronary artery aneurysm at its peak ($t=0.2$ s) for the four models.

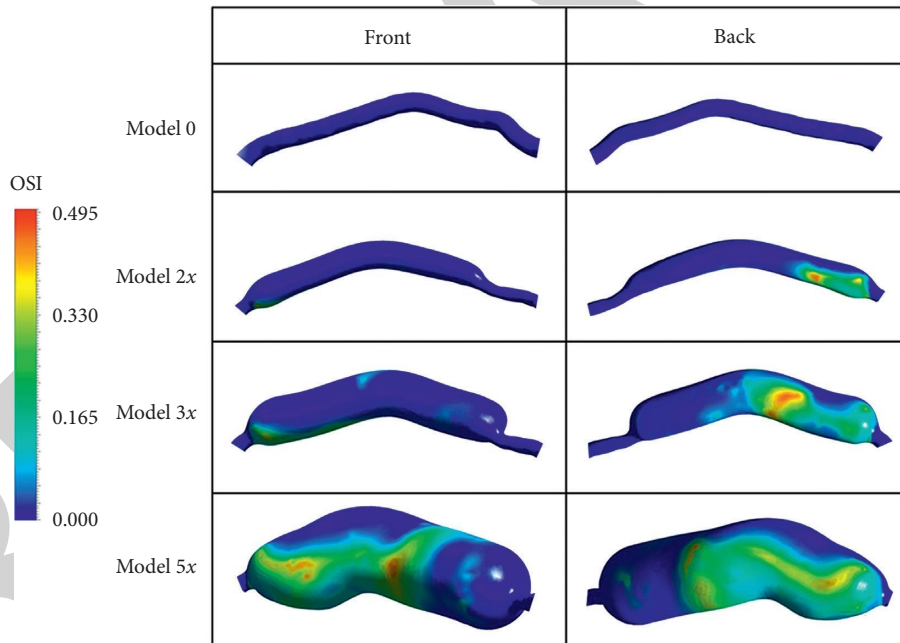


FIGURE 7: Oscillatory shear index (OSI) distribution in the coronary artery aneurysm for the four models.

TABLE 3: The area of high OSI and RRT in the aneurysm and the area of aneurysm.

	Model 0	Model 2x	Model 3x	Model 5x
High OSI area/CAA area (mm^2) (ratio)	0/463.62 (0%)	95.29/762.38 (12.5%)	298.53/1179.97 (25.3%)	1413.89/2135.79 (66.2%)
High RRT area/CAA area (mm^2) (ratio)	0/463.62 (0%)	38.12/762.38 (0.5%)	319.77/1179.97 (27.1%)	1678.73/2135.79 (78.6%)

associated with risk of thrombosis, and that is a more predictive factor of thrombosis than aneurysm diameter [36]. We confirmed that hemodynamic research is beneficial for aneurysm diagnosis and treatment [37]. Therefore, in

this study, we quantitatively calculated the hemodynamic parameters of CAA of different diameters in order to estimate the relationship between the risk level of thrombosis and the size of CAA. The results showed that CAAs only

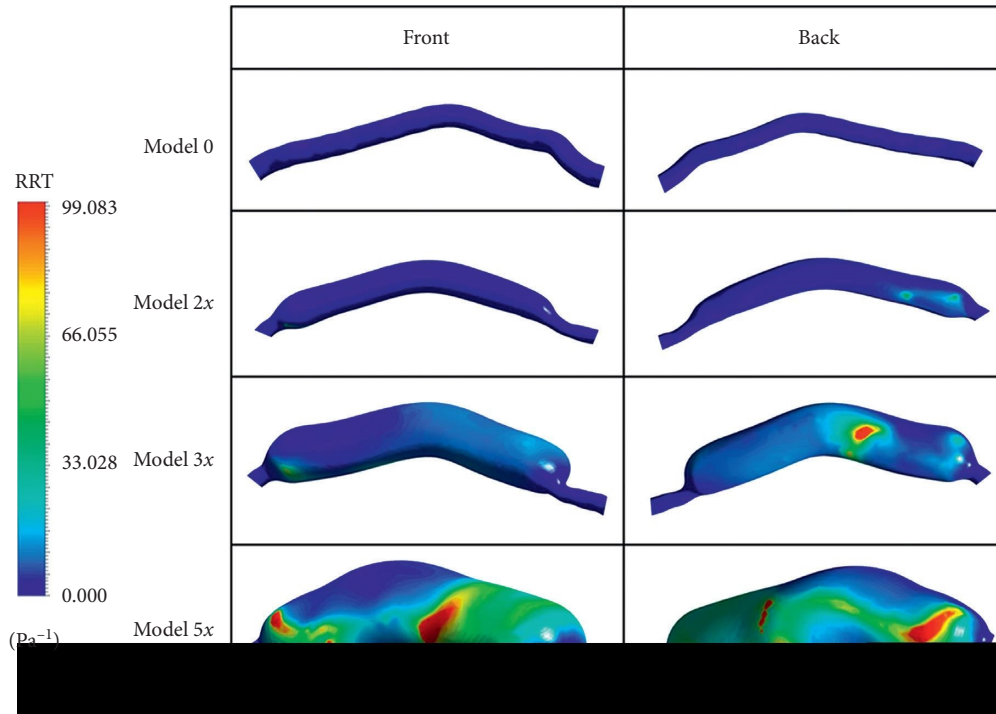


FIGURE 8: Relative residence time (RRT) distribution in the coronary artery aneurysm for the four models.

affect the blood flow and pressure within the region of the lesion itself, with little effect on global blood flow. However, there were substantial changes in local hemodynamic parameters related to thrombosis in the lesion location. Compared with the model without a lesion, all three CAA models showed low WSS, high OSI, and high RRT, with these changes exacerbated as the CAA diameter increased. These changes were the results of the sudden increase in the diameter of the lumen on entering the CAA. These results suggest there may be a high correlation between CAA diameter and the risk of thrombosis. CAA hemodynamic studies may therefore allow the development of a preliminary classification of the risk of thrombosis, helping to improve the effectiveness of anticoagulation therapy and facilitating better personalization of treatment according to a quantitative hemodynamic plan.

Simulation provides a powerful and effective method for estimating important hemodynamic parameters that are difficult to measure. As mentioned above, except mass-flow rate which can be easily detected by non-invasive ultrasound, other parameters, WSS, OSI, and RRT, cannot be directly measured which are usually obtained through in vitro experiments or indirect measurements. Simulation is a non-invasive way, providing a low cost way and avoiding the potential risk of some invasive ways to obtain hemodynamic parameters.

LPM boundary conditions can provide realistic physiologic flow conditions, as what has been confirmed in previous studies [38, 39]. In addition, the coronary microcirculation was introduced into the downstream boundary condition via the LPM. Resistance and pressure changes downstream of the coronary artery could be

accurately captured in this way, helping to ensure the accurate simulation of physiological conditions in the coronary artery. There was no difference between the models in the peripheral vascular structure, so the CFD models shared the same LPM, minimizing the impact of factors other than the diameter of the CAA. Thus, the differences in results between the models were due to the differences in CAA diameters.

As the diameter of the CAA increased, the WSS in the CAA lesion area progressively decreased, with the WSS in Model 5x observed to be >10 times lower than that of the normal coronary artery (Model 0). Parallel plate flow experiments have shown that a large number of platelets accumulate at locations with low WSS (<0.4 Pa) [40], and animal endothelial cell experiments have shown that thrombosis is associated with a decrease in WSS to within the range 0.0770.279 Pa [10]. In the present study, the area average values for WSS in Models 3x and 5x were within this range, suggesting that CAAs with diameters >3 times that of the normal artery are likely to carry a high risk of thrombosis. Although the area average WSS for Model 2x was much lower than that of the model without CAA, it was higher than 0.4 Pa, suggesting that CAAs with diameters double that of the normal artery may not be at high risk of thrombosis. Another important pathophysiological factor in vascular disease is endothelial dysfunction. Low WSS can locally inhibit the production of certain important substances such as NO [41]. An abnormal response to vasodilation agents, including the deactivation of NO by free radicals due to the impairment of acetylcholine or endothelial NO synthase, can lead to abnormal vasoconstriction, which can be associated with endothelial dysfunction [41]. In addition, platelets are prone to aggregation in areas of low WSS, which further

exacerbates the risk of thrombosis. WSS in the CAA lesion of Model 2x was lower than that in the normal model; however, further development is still to be studied just taking WSS as a reference. The risk for thrombosis in CAAs progresses with increasing diameter, so the risk associated with Model 2x would be lower than that for Models 3x and 5x. The development of CAAs needs further study. Although studies have investigated the association between WSS and thrombosis, the current understanding is not yet comprehensive. Therefore, the possibility of WSS and thrombosis in the corresponding in vitro experiments should be the focus of continued research.

The OSIs for the CAAs increased rapidly with increasing diameter of the lesion, with the OSI in Model 5x around 30 times greater than that of the normal coronary artery (which was close to zero throughout the CAA). Previous studies have pointed out that when OSI is greater than 0.2, it will cause endothelial cell damage [31]. The high OSI area (OSI > 0.2) ratio increased from 0.1% to 66.2% between Model 0 and Model 5x. In vivo experimental studies of porcine aortas have reported that disturbed flow (i.e., an increase in OSI) promoted the expression of proinflammatory cytokines in endothelial cells [11]. In addition, an in vitro study of bovine endothelial cells reported that the expression of monocyte chemoattractant protein-1 could be induced by applying a low-amplitude oscillating shear stress of 0.3 Pa at 1 Hz (equivalent to an OSI of 0.5), and this hemodynamic environment enhanced the binding of endothelial cells to monocytes [42]. These findings suggest that the elevated OSI values observed in the CAA models may be associated with conditions that can trigger thrombosis.

The RRT values for the CAAs increased dramatically with increasing diameters of the lesions, with the RRT for Model 5x > 100 times greater than that of the normal coronary artery. The high RRT area ratio increased from 0.1% to 78.6% between Model 0 and Model 5x. These findings indicate that the blood flow in the CAA recirculates when the diameter of the lumen increases, resulting in prolonged contact time between the CAA wall and the blood. Studies have reported a significantly increased risk of thrombosis when RRT is > 10 Pa⁻¹ [12, 34]. The RRT values for Models 3x and 5x in the present study were both > 10 Pa⁻¹, suggesting a high risk of thrombosis when the diameter of a CAA exceeds three times that of the normal coronary artery. Conversely, the RRT for Model 2x was much lower than 10 Pa⁻¹, suggesting that the risk of thrombosis may be low when the diameter of the CAA is only double that of the normal artery. Although there have been various studies of the relationship between RRT and aneurysms [43], the current state of knowledge remains insufficient for patient classification; for example, there are no appropriate ranges of RRT values for distinguishing the risk level of thrombosis which needs further study.

In summary, the comparison of our modeling results with the findings of previous studies suggested that the low WSS, high OSI, and high RRT observed in the CAAs would significantly increase the risk of thrombosis. However, the risk varied considerably between the different diameters of CAA. The WSS, OSI, and RRT values for Models 3x and 5x all suggested a high risk of thrombosis, based on the previous study results. Thus, for CAAs with diameters > 3 times that of

the normal coronary artery, the risk of uncertainty with conservative treatment may be higher than the risk associated with surgery, suggesting that the surgical operation should be considered. Conversely, although the WSS, OSI, and RRT values for Model 2x were unfavorable compared with those of the model of the normal coronary artery, implying an increased risk of thrombosis, the magnitude of these differences was insufficient to support a prediction of the future development of the CAA. For CAAs with a diameter up to two times that of the normal coronary artery, conservative drug treatment may be the better option, avoiding the risks associated with surgery.

The limitations of this study are as follows. First, this study has only one patient's data, and the conclusion may be accidental. We need to use more data for research. Secondly, an important assumption used in the CFD calculation is the rigid wall, where, in fact, elastic walls should be used. In particular, the coronary artery will deform greatly as the heart contracts which can be solved by two-way FSI in the future.

5. Conclusion

The evaluation of the relationship between hemodynamic effects and different diameters of CAAs was performed in this research through the CFD simulation method. The relationship between thrombosis risk and the size of the CAA diameter could be preliminarily evaluated from a hemodynamic perspective.

We found that as the diameter of the CAA increased, the risk of thrombosis increased substantially. The results suggested that when the diameter of a CAA is small (less than double that of the normal coronary artery), the risk of thrombosis may be relatively low, suggesting that medication may be a sufficient approach for the patient, avoiding the uncertain risks associated with surgery. If the diameter of CAA is large (> 3 times that of the normal coronary artery), there may be a high risk of thrombosis, and surgical treatment could be considered. A similar approach could be taken in future studies to systematically assess the risk associated with different shapes, sizes, and locations of aneurysms. Such approaches may form the basis for more sophisticated hemodynamic-based risk stratification methods supporting clinical decision-making in assessment of CAA.

Data Availability

The data used to support the findings of this study are available from the corresponding author upon request.

Conflicts of Interest

The authors declare no conflicts of interest.

Acknowledgments

This research was supported by the National Natural Science Foundation of China (nos. 11832003 and 11772016) and JSPS KAKENHI under Grant no. JP18K18355. This research was partially supported by the Creation of a Development

Platform for Implantable/Wearable Medical Devices by a Novel Physiological Data Integration System of the Program on Open Innovation Platform with Enterprises, Research Institute and Academia (OPERA) from the Japan Science and Technology Agency (JST). This research was also supported by Collaborative Research Project 2020, Institute of Fluid Science, Tohoku University (J20R001) with the Grant Number JP18K18355.

References

- [1] H. Kato, T. Sugimura, T. Akagi et al., "Long-term consequences of kawasaki disease," *Circulation*, vol. 94, no. 6, pp. 1379–1385, 1996.
- [2] S. A. Sherif, O. O. Tok, Ö. Taşköylü, O. Goktekin, and I. D. Kilic, "Coronary, artery aneurysms: a review of the epidemiology, pathophysiology, diagnosis, and treatment," *Frontiers in Cardiovascular Medicine*, vol. 4, 2017.
- [3] E. Beckmann, S. Rustum, S. Marquardt et al., "Surgical treatment of coronary artery aneurysms," *Journal of Cardiac Surgery*, vol. 32, no. 11, pp. 674–679, 2017.
- [4] M. Syed, M. Lesch, and A. D. Syed, "Coronary artery aneurysm: a review," *Progress in Cardiovascular Diseases*, vol. 40, no. 1, pp. 77–84, 1997.
- [5] G. G. Hartnell, B. M. Parnell, and R. B. Pridie, "Coronary artery ectasia. Its prevalence and clinical significance in 4993 patients," *British Heart Journal*, vol. 54, no. 4, 1985.
- [6] A. Satran, B. A. Bart, C. R. Henry et al., "Increased prevalence of coronary artery aneurysms among cocaine users," *Circulation*, vol. 111, no. 19, pp. 2424–2429, 2005.
- [7] O. Topaz, M. S. Rutherford, S. M. Bojack et al., "Giant aneurysms of coronary arteries and saphenous vein grafts: angiographic findings and histopathological correlates," *Cardiovascular Pathology*, vol. 14, no. 6, pp. 298–302, 2005.
- [8] A. P. Antoniadis, Y. S. Chatzizisis, and G. D. Giannoglou, "Pathogenetic mechanisms of coronary ectasia," *International Journal of Cardiology*, vol. 130, no. 3, pp. 335–343, 2008.
- [9] J. B. Gordon, A. M. Kahn, and J. C. Burns, "When children with kawasaki disease grow up," *Journal of the American College of Cardiology*, vol. 54, no. 21, pp. 1911–1920, 2009.
- [10] P. Sriramarao, L. Languino, and D. Altieri, "Fibrinogen mediates leukocyte-endothelium bridging in vivo at low shear forces," *Blood*, vol. 88, no. 9, pp. 3416–3423, 1996.
- [11] A. G. Passerini, D. C. Polacek, C. Shi et al., "Coexisting proinflammatory and antioxidative endothelial transcription profiles in a disturbed flow region of the adult porcine aorta," *Proceedings of the National Academy of Sciences*, vol. 101, no. 89, pp. 2482–2487.
- [12] U. Morbiducci, D. Gallo, R. Ponzini et al., "Quantitative analysis of bulk flow in image-based hemodynamic models of the carotid bifurcation: the influence of outflow conditions as test case," *Annals of Biomedical Engineering*, vol. 38, no. 12, pp. 3688–3705, 2010.
- [13] T. Ohkubo, R. Fukazawa, E. Ikegami, and S. Ogawa, "Reduced shear stress and disturbed flow may lead to coronary aneurysm and thrombus formations," *Pediatrics International*, vol. 49, no. 1, pp. 1–7, 2007.
- [14] H. Anzai, T. Watanabe, X. Han et al., "Endothelial cell distributions and migration under conditions of flow shear stress around a stent wire," *Technology and Health Care*, vol. 28, no. 4, pp. 345–354, 2020.
- [15] M. Zhang, Y. Li, X. Zhao et al., "Haemodynamic effects of stent diameter and compaction ratio on flow-diversion treatment of intracranial aneurysms: a numerical study of a successful and an unsuccessful case," *Journal of Biomechanics*, vol. 58, pp. 179–186, 2017.
- [16] H. Anzai, B. Chopard, and M. Ohta, "Combinational optimization of strut placement for intracranial stent using a realistic aneurysm," *Journal of Flow Control, Measurement & Visualization*, vol. 2, no. 2, pp. 67–77, 2014.
- [17] J. P. Ku, M. T. Draney, F. R. Arko et al., "In vivo validation of numerical prediction of blood flow in arterial bypass grafts," *Annals of Biomedical Engineering*, vol. 30, no. 6, pp. 743–752, 2002.
- [18] A. R. Soler, F. Kabinejadian, M. A. Slevin, P. J. Bartolo, and A. Keshmiri, "Optimisation of a novel spiral-inducing bypass graft using computational fluid dynamics," *Scientific Reports*, vol. 7, no. 1, p. 1865, 2017.
- [19] H. Zhang, L. Li, C. Cheng, and X. Sun, "Clinical value of homodynamic numerical simulation applied in the treatment of cerebral aneurysm," *Experimental and Therapeutic Medicine*, vol. 4, no. 6, pp. 5401–5494, 2017.
- [20] A. S. Les, S. C. Shadden, C. A. Figueroa et al., "Quantification of hemodynamics in abdominal aortic aneurysms during rest and exercise using magnetic resonance imaging and computational fluid dynamics," *Annals of Biomedical Engineering*, vol. 38, no. 4, pp. 1288–1313, 2010.
- [21] M. Piccinelli, A. Veneziani, D. A. Steinman, A. Remuzzi, and L. Antiga, "A framework for geometric analysis of vascular structures: application to cerebral aneurysms," *IEEE Transactions on Medical Imaging*, vol. 28, no. 8, pp. 1141–1155, 2009.
- [22] H. J. Kim, I. E. Vignon-Clementel, J. S. Coogan, C. A. Figueroa, K. E. Jansen, and C. A. Taylor, "Patient-specific modeling of blood flow and pressure in human coronary arteries," *Annals of Biomedical Engineering*, vol. 38, no. 10, pp. 3195–3209, 2010.
- [23] C. A. Taylor, T. A. Fonte, and J. K. Min, "Computational fluid dynamics applied to cardiac computed tomography for noninvasive quantification of fractional flow reserve," *Journal of the American College of Cardiology*, vol. 61, no. 22, pp. 2233–2241, 2013.
- [24] I. E. V. Clementel, C. A. Figueroa, K. E. Jansen, and C. A. Taylor, "Outflow boundary conditions for 3D simulations of non-periodic blood flow and pressure fields in deformable arteries," *Computer Methods in Biomechanics and Biomedical Engineering*, vol. 13, no. 5, pp. 625–640, 2010.
- [25] N. Stergiopoulos, J. J. Meister, and N. Westerhof, "Determinants of stroke volume and systolic and diastolic aortic pressure," *The American Journal of Physiology*, vol. 270, no. 6, pp. 2050–2059, 1996.
- [26] M. Zamir, P. Sinclair, and T. H. Wonnacott, "Relation between diameter and flow in major branches of the arch of the aorta," *Journal of Biomechanics*, vol. 25, no. 11, pp. 1303–1310, 1992.
- [27] K. Johnson, P. Sharma, and J. Oshinski, "Coronary artery flow measurement using navigator echo gated phase contrast magnetic resonance velocity mapping at 3.0 tesla," *Journal of Biomechanics*, vol. 41, no. 3, pp. 595–602, 2008.
- [28] F. P. Salvuccia, C. A. Perazzob, S. Sallesa, J. G. Barrac, and R. L. Armentano, "Influence of inlet conditions in wall shear stress distributions of left coronary arteries in patient-specific simulations," *Mecánica Computacional*, vol. XXIX, pp. 5953–5960, 2010.
- [29] B. C. Lopez, B. Calvo, and P. Estefanía, *Patient-Specific Computational Modeling*, Springer, Berlin, Germany, 2012th edition, 2012.

- [30] D. N. Ghista and F. Kabinejadian, "Coronary artery bypass grafting hemodynamics and anastomosis design: a biomedical engineering review," *BioMedical Engineering Online*, vol. 12, no. 129, 2013.
- [31] F. P. Glor, F. P. Glor, B. Ariff et al., "Image-based carotid flow reconstruction: a comparison between MRI and ultrasound," *Physiological Measurement*, vol. 25, no. 6, pp. 1495–1509, 2004.
- [32] S.-W. Lee, L. Antiga, and D. A. Steinman, "Correlations among indicators of disturbed flow at the normal carotid bifurcation," *Journal of Biomechanical Engineering*, vol. 131, no. 6, Article ID 061013, 2009.
- [33] H. A. Himburg, "Spatial comparison between wall shear stress measures and porcine arterial endothelial permeability," *AJP: Heart and Circulatory Physiology*, vol. 286, no. 5, pp. 1916–1922, 2004.
- [34] T. Suess, J. Anderson, L. Danielson et al., "Examination of near-wall hemodynamic parameters in the renal bridging stent of various stent graft configurations for repairing visceral branched aortic aneurysms," *Journal of Vascular Surgery*, vol. 64, no. 3, pp. 788–796, 2016.
- [35] H. Zhang, X. Yu, F. Ji, and F. Sun, "Coronary artery aneurysm formation after drug-coated," *Medicine*, vol. 97, no. 45, 2018.
- [36] N. G. Gutierrez, M. Mathew, B. W. McCrindle et al., "Hemodynamic variables in aneurysms are associated with thrombotic risk in children with Kawasaki disease," *International Journal of Cardiology*, vol. 281, pp. 15–21, 2019.
- [37] C. Karmonik, G. Chintalapani, T. Redel et al., "Hemodynamics at the ostium of cerebral aneurysms with relation to post-treatment changes by a virtual flow diverter: a computational fluid dynamics study," in *Proceedings of the Annual International Conference of the IEEE Engineering in Medicine and Biology Society, EMBS*, pp. 1895–1898, Osaka, Japan, July 2013.
- [38] J. T. Marcus, H. G. Smeenk, J. P. A. Kuijter, R. J. Van Der Geest, R. M. Heethaar, and A. C. Van Rossum, "Flow profiles in the left anterior descending and the right coronary artery assessed by MR velocity quantification: effects of through-plane and in-plane motion of the heart," *Journal of Computer Assisted Tomography*, vol. 23, no. 4, pp. 567–576, 1999.
- [39] Y. Shi, P. Lawford, and R. Hose, "Review of zero-D and 1-D models of blood flow in the cardiovascular system," *Bio-Medical Engineering Online*, vol. 10, no. 1, p. 33, 2011.
- [40] M. Kroll, J. Hellums, L. McIntire, A. Schafer, and J. Moake, "Platelets and shear stress," *Blood*, vol. 88, no. 5, pp. 1525–1541, 1996.
- [41] J.-J. Chiu and S. Chien, "Effects of disturbed flow on vascular endothelium: pathophysiological basis and clinical perspectives," *Physiological Reviews*, vol. 91, no. 1, pp. 327–387, 2011.
- [42] J. Hwang, M. H. Ing, A. Salazar et al., "Pulsatile versus oscillatory shear stress regulates NADPH oxidase subunit expression," *Circulation Research*, vol. 93, no. 12, pp. 1225–1232, 2003.
- [43] S.-i. Sugiyama, K. Niizuma, T. Nakayama et al., "Relative residence time prolongation in intracranial aneurysms," *Neurosurgery*, vol. 73, no. 5, pp. 767–776, 2013.